Reconstruction of the Fermi surface induced by high magnetic field in the quasi-two-dimensional charge density wave conductor η-Mo_4O_{11}

J. Z. Ke, M. Yang, H. P. Zhu, C. B. Liu, C. Dong, W. X. Liu, M. Y. Shi, and J. F. Wang*

Wuhan National High Magnetic Field Center and School of Physics, Huazhong University of Science and Technology, Wuhan 430074, People's Republic of China

(Received 29 September 2020; revised 19 November 2020; accepted 3 December 2020; published 22 December 2020)

Low-dimensional charge density wave (CDW) systems, which undergo successive so-called Peierls phase transitions at characteristic temperatures associated with corresponding changes in electronic structure, are of great importance for exploring novel quantum physics. Here, we report systematic research of the magneto-transport properties for the quasi-two-dimensional CDW conductor η-Mo_4O_{11} under high magnetic fields up to 59 T. Measurements of in-plane and out-of-plane magnetoresistance and Hall resistance have been carried out to determine the Fermi surface (FS) structure at low temperatures and high magnetic fields. Beyond the quantum limit (QL), fast quantum oscillations (QOs) with complex periods have been found in both MR and Hall resistance, representing a direct measurement of the area of the FS. In addition, we observe a conspicuous phase transition at 45 T. The QO frequency and carrier density successively increase above the QL and phase transition fields. Consequently, we propose that such remarkable feature of the magnetic field dependence of the fast QOs for η-Mo_4O_{11} arises from the field-induced density wave transition and FS reconstruction. We have further discussed the mechanism and provided the evolution on the geometry of the FS with magnetic field in the second CDW state based on the field-dependent FS model.

DOI: 10.1103/PhysRevB.102.245135

I. INTRODUCTION

Over the last two decades, a subject of continued interest is the observations of new quantum oscillations (QOs) and phase transitions induced by high magnetic fields in the magnetoresistance (MR) of low-dimensional conductors, specifically in the anisotropic charge density wave (CDW) systems showing quasi-one-dimensional (1D) or quasi-two-dimensional (2D) lattice structures [1–6]. The molybdenum oxides purple bronze AMo_6O_{17} (A = Na, K) and two phases of Mo_4O_{11} (γ, η) are typical CDW systems arising from the Fermi surface (FS) nesting involved with the Peierls instability [7–15]. It is believed that the nesting of quasi-1D FSs gives rise to the formation of the density wave phase. The concept of FS nesting has dictated the corresponding lattice distortion at low temperatures and introduced a periodic potential with wave vector Q of the CDW, which is distinguished from the mechanisms based on the strong electron-phonon coupling and charge modulation.

In particular, the quasi-2D CDW conductor η-Mo_4O_{11} has attracted considerable attention because of its intriguing properties such as possible quantum Hall effect (QHE), deformation and sliding motion of CDW condensations, and fast QOs beyond the quantum limit (QL) [14–21]. The structure of η-Mo_4O_{11} belongs to the monoclinic space group $P21/c$ and η-Mo_4O_{11} consists of four independent Mo sites occupying a MoO_4 tetrahedron and three MoO_6 octahedrons. The MoO_6 conducting layers are stacked along the a axis via MoO_4 insulating layers [22,23]. Consequently, η-Mo_4O_{11}, whose electronic properties are highly anisotropic in CDW phases, can be considered as a quasi-2D electron system owing to the special crystal structure. Moreover, η-Mo_4O_{11} undergoes successive CDW transitions at characteristic temperatures $T_{c1} = 105$ K and $T_{c2} = 30$ K with different nesting vectors [17,19,24–28]. Band structure calculations within a tight-binding model, Compton scattering, and angle resolved photoemission spectroscopy (ARPES) measurements have revealed that the original electron and hole FSs in the normal metal phase occupy 25% of the first Brillouin zone (BZ). There are two equivalent "V-shaped" hole FSs (∼12.5% × 2) and hexagonal electron FSs (∼25%) located around the Y points and the Γ point in the BZ, respectively [24,25,29]. In early transport studies, Hill *et al.* reported the possibility of anomalous bulk quantum Hall effect (QHE)-like plateaus in η-Mo_4O_{11} caused by the imperfectly nested CDW and the exchange of carriers between these mobile states and localized CDW condensation [18], whereas other mechanisms of the possible QHE based on a 2D chiral-surface-state have also been proposed [14]. Furthermore, Sasaki *et al.* claimed the magnetic field induced CDW-to-normal phase transition and sliding motion of the CDW connected with the CDW-gap narrowing of the nested electron and hole bands in this compound [16]. Nevertheless, the ultrahigh-field transport behaviors about the fast QOs observed beyond the QL in η-Mo_4O_{11} still remain puzzling [26], and a similar phenomenon has also been reported in the quasi-2D organic conductor $(BEDF\text{-}TTF)_2KHg(SCN)_2$ [30–32]. Therefore, complete determination of the mechanism for the fast QO beyond the QL in η-Mo_4O_{11} will be necessary at

*jfwang@hust.edu.cn

 ©2020 American Physical Society

present to understand the related intriguing quantum phenomena. Indeed, the fascinating behaviors under magnetic fields have proven to be extremely valuable to explore and even manifest the high-field properties in CDW systems. This motivated us to investigate the high-field FS structure of η-Mo_4O_{11} by performing systematic quantum transport measurements.

In this paper, we present a comprehensive study of in-plane and out-of-plane MR and Hall resistance for η-Mo_4O_{11} single crystals under pulsed magnetic field up to 59 T. Above the QL (19 T), fast QOs with complex frequencies have been found in both MR and Hall resistance, allowing for direct exploration and study of FS properties. At a higher field of 45 T, we have observed a pronounced phase transition of a sudden increase in interlayer MR. In addition, the fast QOs show increasing periodicities depending on magnetic field range and Hall resistance exhibits a corresponding tendency towards zero, implying that the carrier density increases with magnetic field. Based on these results, we have presented an interpretation of the evolution of the FS with magnetic field from the fast QOs in the high-field phase. To consider this model, we suggest that the field-dependent FS is responsible for the unique quantum behaviors observed beyond the QL. The striking QO features thus signify a previously unknown reconstructed FS topology in the high-field state with several revived "nested or vanishing" bands, leading to a good understanding of its quasi-2D nature and providing an ideal platform to investigate other exotic physical phenomena in the CDW system.

II. EXPERIMENT

Single crystals of η-Mo_4O_{11} used in the study were prepared by a standard chemical vapor transport (CVT) method using MoO_2 and MoO_3 in a molar ratio of 1:3.1 as the starting materials with $TeCl_4$ or I_2 as carrier gas, which has been reported in our previous work [33]. The as-grown crystals were checked using powder x-ray diffraction (XRD) and cut into thin plates optimized for transport measurements with dimensions of $\sim 2 \times 0.5 \times 0.08\,mm^3$. The orientations of the single crystals were confirmed by single-crystal XRD technique. The sample was aligned with the a axis along the magnetic field in all experiments. The low-field electrical transport measurements were carried out using a commercial physical property measurement system (PPMS). The high-field transport measurements with five-probe method were performed by a pulsed magnet up to 59 T with pulse duration of 150 ms at the Wuhan National High Magnetic Field Center (WHMFC). The contact resistances were maintained to be smaller than 1 Ω and the amplitude of the current was 1 mA in all measurements, which is important to obtain good signal-to-noise ratio and avoid the heating effect in the pulsed magnetic field.

III. RESULTS AND DISCUSSION

Figure 1(a) shows the temperature dependence of the resistivity ρ for η-Mo_4O_{11} at zero magnetic field. The current directions are parallel to the b axis for ρ_{xx} and the a axis for ρ_{zz}. Consistent with earlier reports [17,19], η-Mo_4O_{11} undergoes two obvious metal-to-metal transitions at $T_{c1} = 105$ K and $T_{c2} = 30$ K, respectively, which are characteristic for the

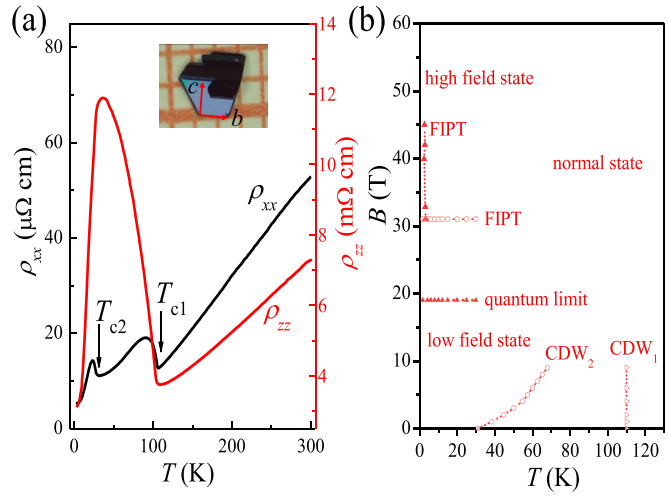

FIG. 1. (a) Temperature dependence of the resistivity ρ for η-Mo_4O_{11} with decreasing temperature. The current directions are parallel to the b axis for ρ_{xx} (black line) and the a axis for ρ_{zz} (red line). Black arrows indicate the CDW transition temperatures $T_{c1} = 105$ K and $T_{c2} = 30$ K, respectively. The inset of (a) shows the typical crystal that exhibits a characteristic morphology with natural (100) facet. The red arrows in the inset mark the corresponding crystallographic directions of the grown crystal in the bc plane. (b) The B-T phase diagram with several characteristic fields at different temperatures. "FIPT" denotes the field-induced phase transition.

CDW transitions in a quasi-2D material. Since most of the original FSs are destroyed at the two CDW transitions, the compound thus consists of only several small electron and hole pockets and two types of CDW condensation at low temperatures [24,25,29]. The inset of Fig. 1(a) presents the typical crystal, which shows a characteristic morphology with natural (100) facet confirmed by the single-crystal XRD technique [33]. In Fig. 1(b), the B-T phase diagram for η-Mo_4O_{11} is displayed with several characteristic fields at different temperatures. The phase transitions above 9 T are determined from the pulsed magnetic field data indicated by arrows in Fig. 2, and the phase boundary below 9 T is derived from our PPMS measurements shown in the Supplemental Material [34]. The second critical temperature T_{c2} increases monotonically with magnetic field owing to the orbital coupling effect [4,35], whereas the first critical temperature T_{c1} shows no change with magnetic field up to 9 T; these are appended to the Supplemental Material, Fig. S1 [34]. Note that the phase diagram is extracted from both the in-plane and out-of-plane MR measurements, as will be concretely discussed in the following sections.

In Fig. 2(a), we show the ρ_{xx}, ρ_{xy}, and ρ_{zz}, respectively, at $T = 1.4$ K as a function of magnetic field B up to 59 T. All the observations of low-field ρ_{xx}, ρ_{xy}, and ρ_{zz} are in agreement with previous measurements on these in static magnetic fields using PPMS [33]. The ρ_{xx} and ρ_{zz} increase with B accompanying the low-frequency ($f_{\rm low} = 19$ T) Shubnikov–de Haas (SdH) oscillations superimposed on the MR background [33]. The low-frequency carrier will enter the QL at sufficiently high fields, where all carriers occupy only the lowest-energy Landau level. Meanwhile, the ρ_{xy} shows a maximum around 11 T [33]. With magnetic field up to

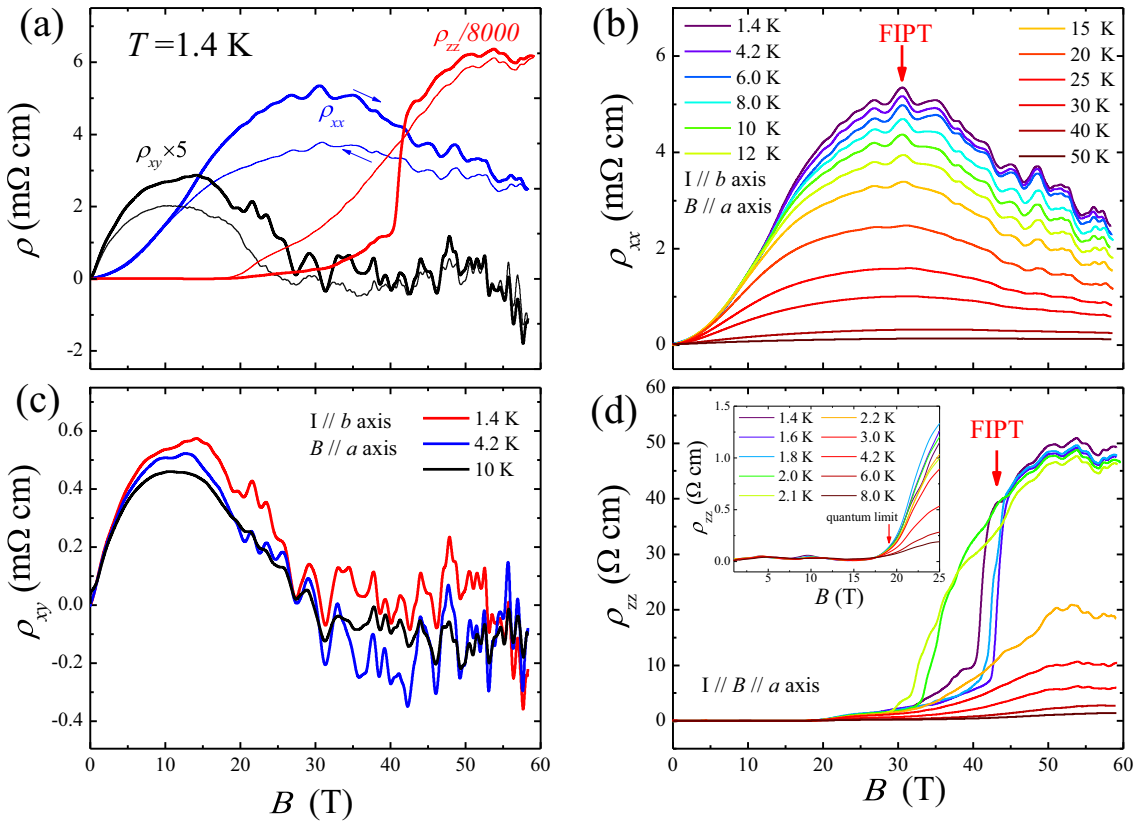

FIG. 2. Magnetic field dependence of (a) ρ_{xx} (blue line), ρ_{xy} (yellow line), and ρ_{zz} (red line) at $T = 1.4$ K and with magnetic field up to 59 T, respectively. Note that ρ_{xy} has been amplified 5 times and ρ_{zz} has been reduced by 8000 times for clarity. The thick line is for the ascending field and the thin line is for the descending field. All the curves shown below are up-sweep ones. (b) Detailed ρ_{xx} at various temperatures from 1.4 to 50 K. The red arrow indicates the maximum MR. (c) ρ_{xy} at 1.4, 4.2, and 10 K. (d) ρ_{zz} from 1.4 to 8 K. The inset of (d) displays the low-field results of ρ_{zz} as $B < 25$ T. The red arrows mark two characteristic fields of the QL and FIPT, respectively.

59 T, the ρ_{xx} continues to increase distinguishably until 31 T, after which it presents a gradually decreasing behavior. On the other hand, the ρ_{xy} drops rapidly from the maximum and shows a tendency towards zero, indicating the increasing carrier density with magnetic field. In addition, a striking phase transition with the dramatic increase in ρ_{zz} is uncovered at the characteristic magnetic field (defined as $B_{\rm PT} = 45$ T). Notably, both MR and Hall resistance curves exhibit fast QO character even above QL field (defined as $B_{\rm QL} = 19$ T), which thus cannot be assigned to the conventional SdH effect. Moreover, as presented in Fig. 2(a), all the curves show a complicated hysteresis between up-sweeps and down-sweeps of the magnetic field as reported previously [15,16,26]. In fact, similar hysteresis character has been widely observed in its brother compound KMo_6O_{17} and other low-dimensional spin density wave (SDW) Bechgaard salt systems [36–38]. The hysteresis is associated with a first-order phase transition and ascribed to the CDW nesting wave vector shifting as the field-induced SDW and CDW hybrid state transition emerges in the falling sweep [4,26,39]. It should be stressed that the hysteresis behavior gradually vanishes with temperature approaching $T_{c2} = 30$ K. The same as in previous studies [19,20], only the data for the rising field part are presented in Figs. 2(b)–2(d) for simplicity because the QO analyses are consistent between rising and falling field sweeps. Figure 2(b) shows the detailed magnetic field dependence of ρ_{xx} across a wide temperature range from 1.4 to 50 K. Fast QOs decrease in amplitude with increasing temperature and finally disappear as $T > T_{c2}$. Another feature is the existence of an anomaly at $B = 31$ T (maximum MR). The decreasing behavior of ρ_{xx} above 31 T can be connected with the suppressing effect of strong magnetic fields on the CDW, indicative of the transition into another field-induced phase. Figure 2(c) shows magnetic field dependence of ρ_{xy} at temperatures of 1.4, 4.2, and 10 K. Figure 2(d) shows magnetic field dependence of ρ_{zz} from 1.4 to 8 K. The inset of Fig. 2(d) demonstrates the corresponding low-field results of ρ_{zz} as $B < 25$ T. Moreover, the phase transition found at B_{PT} is distinct accompanied with a shape increase in ρ_{zz} as $T < 2.1$ K, and extremely sensitive to temperature, which may be relevant to an abrupt change in the anisotropy of the temperature-dependent scattering time on the bands.

In order to discuss the electronic structure of η-Mo_4O_{11} in the high-field state, we extracted the oscillation component $\Delta\rho$ after subtracting a smoothed background. As presented in Figs. 3(a) and 3(b), the $\Delta\rho_{xx}$ and $\Delta\rho_{zz}$ above the $B_{\rm QL}$ are plotted against $1/B$. Notably, the QOs exhibit many frequencies and the amplitude decreases with increasing temperature. Figures 3(c) and 3(d) display the subsequent fast Fourier transform (FFT) spectra of ρ_{xx} at various temperatures. As $19\,{\rm T} < B < 45\,{\rm T}$, FFT results resolve two main peaks centered at $f_\alpha = 167$ T and $f_\beta = 233$ T,

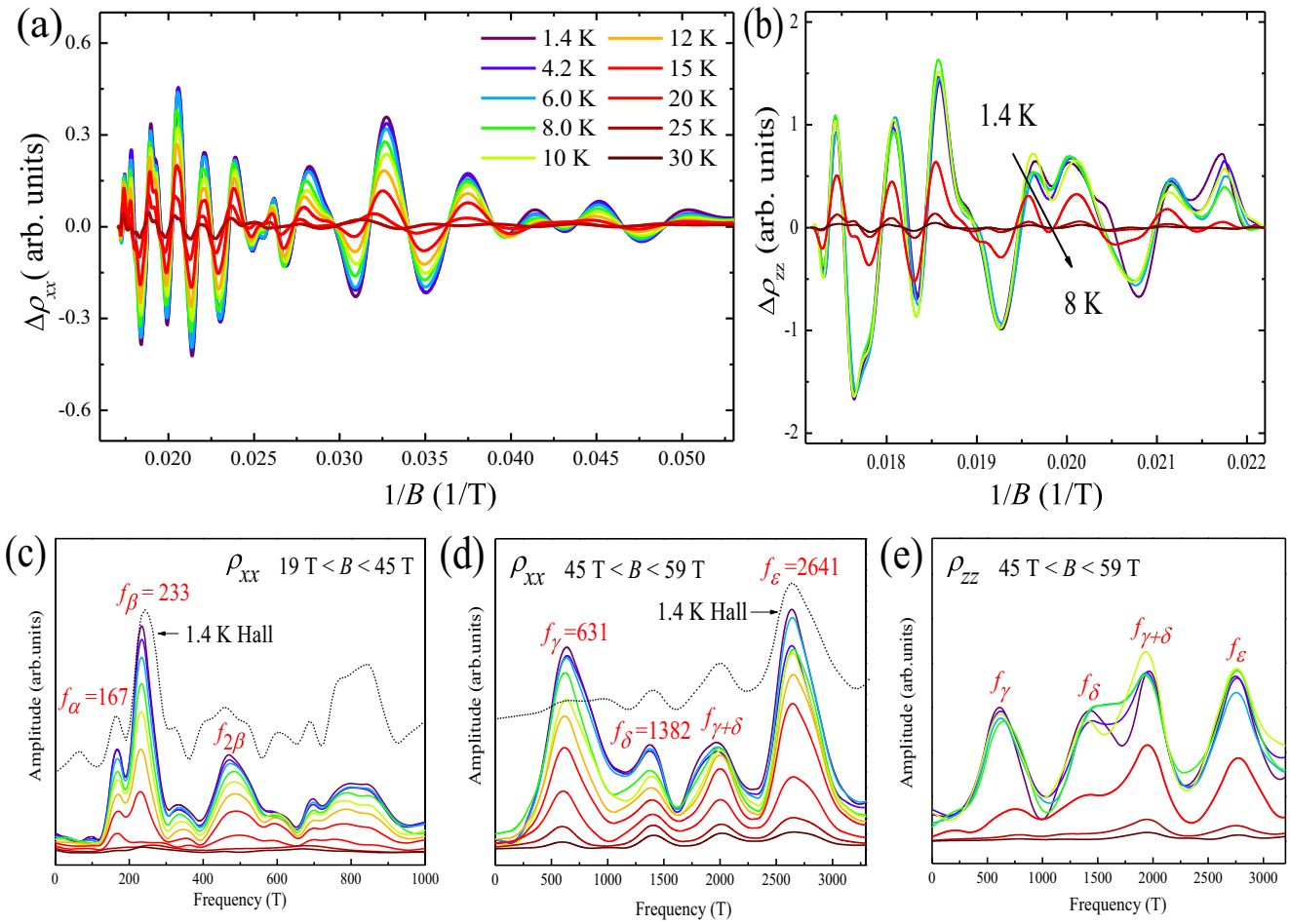

FIG. 3. (a), (b) The high-field oscillation component $\Delta\rho_{xx}$ and $\Delta\rho_{zz}$ plotted against inverse field $1/B$ above the $B_{\rm QL}$ and $B_{\rm PT}$ after subtracting a smoothed background, respectively. (c), (d) The FFT spectra of ρ_{xx} in two field ranges of 19 T $< B <$ 45 T and 45 T $< B <$ 59 T, respectively. The black dotted curves in (c), (d) indicate the FFT results of ρ_{xy} at $T = 1.4$ K over different field ranges. (e) The FFT results of ρ_{zz} as 45 T $< B <$ 59 T.

which have been found by previous work [26] and the harmonics such as 2β have also been detected. For the limited field range 45 T $< B <$ 59 T, we reveal three major frequencies of $f_\gamma = 631$ T, $f_\delta = 1382$ T, and $f_\varepsilon = 2641$ T with their linear combination frequency $\gamma + \delta$, not previously reported. Moreover, the black dotted curves in Figs. 3(c) and 3(d) show the FFT spectra of ρ_{xy} at lowest temperature $T = 1.4$ K for a comparison. The FFT peaking values of ρ_{xy} are almost consistent with that of ρ_{xx}, indicating that the high-field fast QOs of ρ_{xy} and ρ_{xx} have the same origin. Figure 3(e) displays the high-field FFT results of ρ_{zz} where the three frequencies (γ, δ, ε) can also be resolved. The largest frequency f_ε detected above the B_{PT} is more than two orders of magnitude greater than that of the low-field SdH oscillations ($f_{\rm low} = 19$ T) [33]. As we know, the carrier density $n_{\rm 2D}$ can be written as the relationship $n_{\rm 2D} = \upsilon_v \upsilon_s ef/h$ for 2D systems, where e is the elementary charge, υ_s and υ_v denote the spin and valley degeneracy, and h is the Planck constant. Consequently, by taking $\upsilon_s = 2$ and a single valley we can obtain the corresponding carrier densities of different frequencies with $n_a = 8.07 \times 10^{16}\,{\rm m}^{-2}$, $n_\beta = 1.12 \times 10^{17}\,{\rm m}^{-2}$, $n_\gamma = 3.04 \times 10^{17}\,{\rm m}^{-2}$, $n_\delta = 6.67 \times 10^{17}\,{\rm m}^{-2}$, and $n_\varepsilon = 1.27 \times 10^{18}\,{\rm m}^{-2}$, whereas the low-field carrier density with frequency $f_{\rm low} = 19$ T is $9.18 \times 10^{15}\,{\rm m}^{-2}$. Notably, a large number of the conduction carriers are induced significantly as magnetic field far beyond the $B_{\rm QL}$, well corresponding to the unique behavior of the Hall resistance decreasing to zero under high magnetic fields. On the other hand, according to the Lifshitz-Kosevich theory, the oscillation amplitude $\Delta\rho$ can be described by the expression $\Delta\rho/\rho_0 \propto R_T R_D \cos(2\pi f/B)$ where $R_T = \alpha T m^*/B\sinh(\alpha T m^*/B)$ is the thermal damping factor, $R_T = \exp(-\alpha T_D m^*/B)$ is the Dingle damping factor, m^* is the effective mass, T_D is the Dingle temperature, $\alpha = 2\pi^2 k_B m_e/(e\hbar) \sim 14.69\,{\rm T/K}$, k_B is the Boltzmann constant, and m_e is the free-electron mass [40,41]. As a result, the effective mass m^* can be quantified in terms of analyzing the temperature dependence of the FFT peak amplitudes with the relation R_T. The fitted effective mass is shown in Fig. 4 and summarized as follows: $m_\alpha = 0.41\ m_e$, $m_\beta = 0.45\ m_e$, $m_\gamma = 0.52\ m_e$, $m_\delta = 0.54\ m_e$, $m_\varepsilon = 0.46\ m_e$, while the low-field ($B < B_{\rm QL}$) effective mass has been calculated to be less than $0.1\ m_e$ [20,26]. In addition, the extremal cross-section area S of the FS perpendicular to magnetic field, which can be

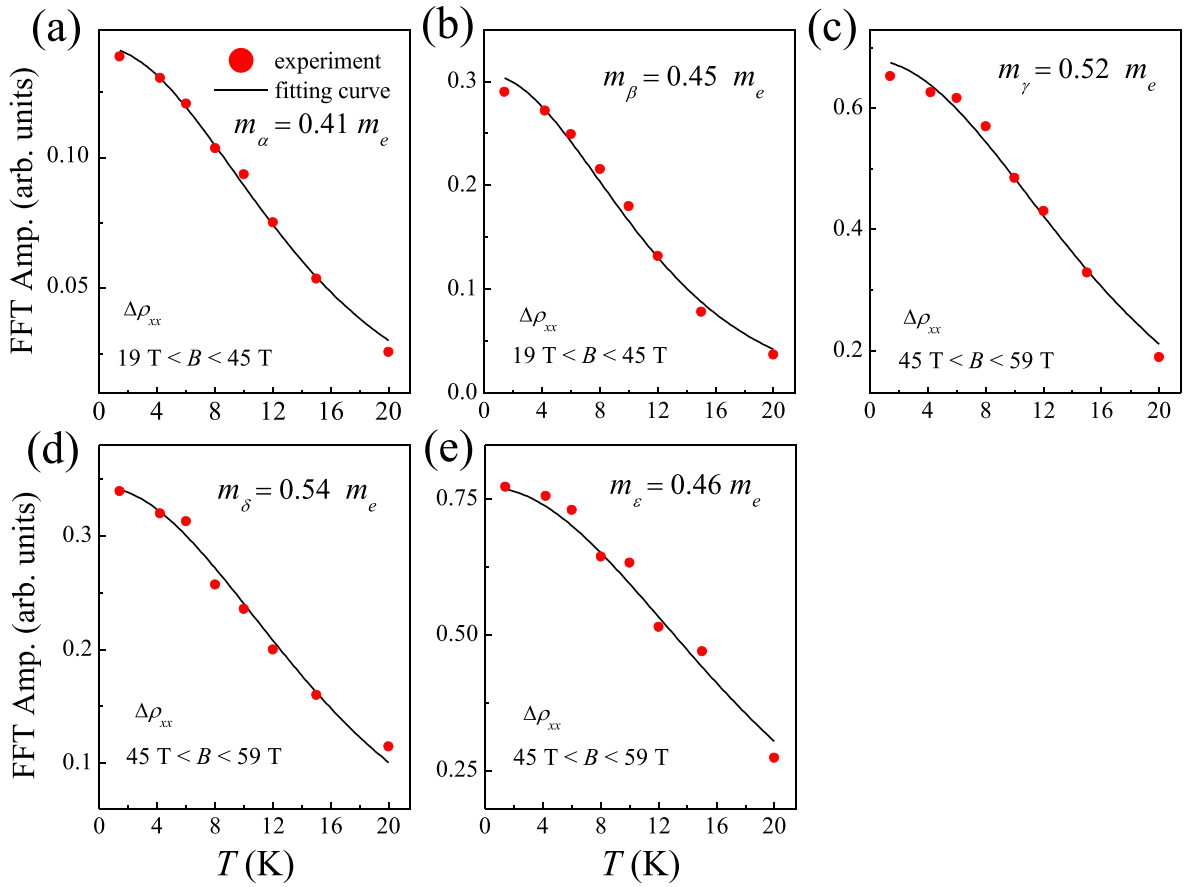

FIG. 4. (a)–(e) The Lifshitz-Kosevich (LK) fitting of the temperature dependence of the FFT amplitudes for different frequencies, respectively. The red dots are the experimental results, and the black solid lines are the fitted results according to the LK formula shown in the main text.

determined by the Onsager relation $S = 4\pi^2 ef/h$, is vital to analyze the QOs. However, according to the previous dynamic transient thermoelectric effect (TTE) study, 70% for original electron FSs and 78% for original hole FSs are destroyed with wave vector $Q_1(0, 0.23b^*, 0)$ at the first CDW transition $T_{c1} = 105$ K [42]. Consequently, the sizes of the electron and hole FSs in the first CDW phase (30 K $< T <$ 105 K) are evaluated to be 7.5% and 2.75% of the BZ, respectively. Since the FSs are further gapped out with the wave vector $Q_2(0.42b^*, 0.28c^*)$ at the second CDW transition, $T_{c2} = 30$ K, the remaining FSs occupy nearly 0.2% of the BZ in the second CDW phase ($T < 30$ K) and are only responsible for the low-field transport properties [24–26,29,42]. In a previous study, the fast QOs with the frequencies f_α and f_β have been found and interpreted in terms of possible Stark quantum interference oscillation coupled with magnetic breakdown [26], which emerges when electrons can pass through two alternative paths between equivalent points in k space and wave functions further interfere with each other [38,43]. However, this Stark effect is unlikely to happen in the quasi-2D η-Mo_4O_{11} since the parallel FSs have been gapped out and the potential "hidden" one dimensionality has completely vanished in the second CDW phase. Moreover, magnetic breakdown would introduce other frequencies manifesting as a beat or nonmonotonic amplitude modulation, which are also absent in our results. Therefore, we would like to attribute the QOs observed in the high-field phase to other origins after excluding the remaining FS pockets as well as Stack quantum interference in the second CDW state. Actually, this scenario is highly reminiscent of the magnetic field induced FS reconstruction extensively reported in cuprate superconductors, SDW organic conductors, heavy-fermion, and Dirac semimetal systems [44–49]. Additionally, based on the detailed calculations, the $f_{\text{low}} = 19$ T corresponds to the FS size about $S_{\text{low}} = 0.2\%$ of the BZ, well consistent with the calculated FS pockets remaining in the second CDW phase. The frequencies f_α, f_β correspond to the FS sizes about $S_\alpha = 1.5\%$ and $S_\beta = 2.1\%$ of the BZ, respectively. The frequencies f_γ, f_δ, and f_ε correspond to the FS sizes of about $S_\gamma = 5.8\%$, $S_\delta = 12.5\%$, and $S_\varepsilon = 23.5\%$ of the BZ. Interestingly, the cross-section S_δ and S_ε can fairly match with the "V-shaped" hole FS (~12.5%) and hexagonal electron FS (~25%) in the normal metal phase, while S_γ can be correlated with the nested portion of electron FS (~7.5%) at the second CDW transition. In view of the detailed data analyses and existing band structure, we thus arrive at a possible explanation for the fast QOs in the high-field phase, originating from the reconstructed FSs caused by field-induced density wave transition, as found in the benchmark bilayer material $YBa_2Cu_3O_{7-x}$ [50]. The reappearance of the "nested or vanishing" FSs and abundant carriers gives rise to the abrupt FS reconstruction, because

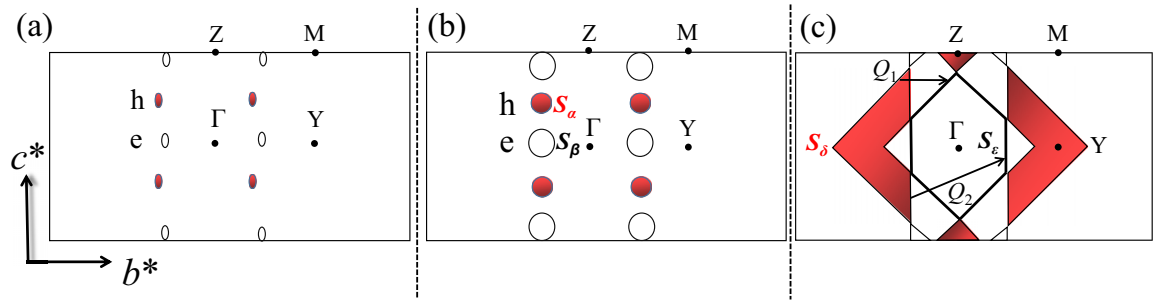

FIG. 5. The schematic pictures of the FS evolution with magnetic field for the quasi-2D CDW conductor η-Mo_4O_{11}. (a) FS image as $B < 19$ T according to the band structure calculations [25]. (b) The estimated FS image as 19 T $< B <$ 45 T. (c) The proposed FS picture as 45 T $< B <$ 59 T. The open and red shaded areas in (a)–(c) denote the electron and hole FSs, respectively. The black arrows in (c) indicate the two wave vectors Q_1 and Q_2, respectively.

of the Pauli paramagnetic coupling between the magnetic field and the charge carrier will lead to a gradual suppression of the CDW with increasing magnetic field as reported in $Li_{0.9}Mo_6O_{17}$ [7]. Besides, since the fast QOs of Hall resistance and MR show nearly identical frequencies, it is reasonable to conclude that they have a common origin of the reconstructed FSs.

Based on the discussion of the high-field data shown above, we can draw the approximate reconstructed 2D FS topology. Figures 5(a)–5(c) present the detailed schematic pictures of the FS evolution for η-Mo_4O_{11} over different magnetic field ranges. Figure 5(a) shows the initial FS picture of combined electron and hole pockets in the second CDW phase according to the previous band structure calculations [25]. The open and red shaded circles covering 0.2% of the BZ indicate the small electron and hole FSs, respectively, that give rise to low-field ($B < B_{QL}$) quantum phenomena. Figure 5(b) shows the estimated FS schematic image in the field range of 19 T $< B <$ 45 T. The corresponding hole and electron FSs occupy $S_\alpha = 1.5\%$ and $S_\beta = 2.1\%$ of the BZ, respectively, owing to the decreasing CDW gap induced by the magnetic field. Similarly, Fig. 5(c) shows the proposed FS schematic picture as 45 T $< B <$ 59 T. The two equivalent "V-shaped" red shaded areas located around the Y points represent the hole FSs with the overall size $2S_\gamma = (12.5\% \times 2)$ of the BZ, and the hexagonal open area located around the Γ point denotes the electron FS with the overall size $S_\varepsilon = 23.5\%$ of the BZ. Actually, the cross-sectional areas of FS based on the frequencies extracted from the FFT of quantum oscillations are consistent with parts of the unreconstructed FS that have previously been revealed by Compton scattering and ARPES experiments [24,29]. To our knowledge, the underlying mechanism of the magnetic field induced FS reconstruction in CDW systems is still under debate and one most probable explanation can be summarized as follows: A strong magnetic field will alter the band structure in terms of the field-induced density wave transitions that arise from an interplay of Zeeman (Pauli) and orbital effects. The superposition of the orbital and Zeeman (Pauli) effects will change the characteristics connected with CDW formations such as critical temperature, order parameter, and nested wave vector [4,35,51]. In particular, the Pauli coupling of magnetic field to charge carrier will suppress the CDW interaction in the high-field state since only the band that has the same spin can be coupled by CDW. However, in an external magnetic field, it is not likely to have the same nested wave vector for both up- and down-spin bands. At some characteristic fields, the CDW energy can be minimized in this case by introducing a field-dependent nested wave vector that can lead to the gapless phase. Thereby, a conventional CDW is not the most advantageous as the Zeeman (Pauli) energy is equal to the condensation energy of CDW in the high-field phase [52–54]. The quasi-1D FS nesting will be reduced with increasing magnetic field and even removed above the B_{PT}. Such coupling effect will reconstruct the FS topology in the high-field phase, resulting in an increasing FS with magnetic field as exhibited in Figs. 5(a)–5(c). This proposed reconstructed FS model can well describe and explain the high-field fast QOs for η-Mo_4O_{11}. Furthermore, the phase diagram presented in Fig. 1(b) for η-Mo_4O_{11} may be quite complicated because the quasi-1D FS nesting is both temperature and magnetic field dependent, and further adequate investigations by other experimental techniques are necessary to enrich the phase diagram. Besides, this field-dependent FS model also gives us an important clue for exploring and uncovering high-field induced exotic physical phenomena that occur beyond the QL in other low-dimensional CDW systems.

IV. CONCLUSION

In conclusion, we have reported the systematic measurements and analysis of the in-plane MR and Hall resistance, and interlayer MR for the quasi-2D CDW conductor η-Mo_4O_{11} under high magnetic field up to 59 T. Above the QL, magnetic field induced fast QOs and phase transition have been observed in these measurements. The QO frequency and carrier density successively increase above the B_{QL} and B_{PT}. These corresponding FS sizes in the high-field state accord well with those of "nested or vanishing" normal metal phase FS. The result well supports the emergence of the unreconstructed FS at high fields as CDW is suppressed. Consequently, we propose a field-dependent FS model where the gapped-out FSs become active in the high-field phase. We further provide the FS topology and evolution with magnetic field for η-Mo_4O_{11}, in satisfactory agreement with the experiment results. Nevertheless, more detailed experiments as well as theoretical studies related to high-field FS structure are desirable to confirm the proposed reconstructed FS model.

ACKNOWLEDGMENTS

This work was supported by the National Natural Science Foundation of China (Grants No. 12004122, No. U1832214, and No. 12074135) and the Fundamental Research Funds for the Central Universities (Grant No. 2018KFYXKJC005).

[1] F. Clerc, C. Battaglia, M. Bovet, L. Despont, C. Monney, H. Cercellier, M. G. Garnier, and P. Aebi, Phys. Rev. B **74**, 155114 (2006).

[2] X. T. Zhu, Y. W. Cao, J. D. Zhang, E. W. Plummer, and J. D. Guo, Proc. Natl. Acad. Sci. USA **112**, 2367 (2015).

[3] M. H. Whangbo, E. Canadell, P. Foury, and J. P. Pouget, Science **252**, 96 (1991).

[4] D. Zanchi, A. Bjelis, and G. Montambaux, Phys. Rev. B **53**, 1240 (1996).

[5] P. D. Grigoriev and D. S. Lyubshin, Phys. Rev. B **72**, 195106 (2005).

[6] G. Montambaux, M. Héritier, and P. Lederer, Phys. Rev. Lett. **55**, 2078 (1985).

[7] X. F. Xu, A. F. Bangura, J. G. Analytis, J. D. Fletcher, M. M. J. French, N. Shannon, J. He, S. Zhang, D. Mandrus, R. Jin, and N. E. Hussey, Phys. Rev. Lett. **102**, 206602 (2009).

[8] O. Sepper and A. G. Lebed, Phys. Rev. B. **90**, 094509 (2014).

[9] P. Mallet, K. M. Zimmermann, P. Chevalier, J. Marcus, J. Y. Veuillen, and J. M. G. Rodriguez, Phys. Rev. B **60**, 2122 (1999).

[10] M. H. Whangbo, E. Canadell, and C. Schlenker, J. Am. Chem. Soc. **109**, 6308 (1987).

[11] H. Guyot, J. Dumas, M. V. Kartsovnik, J. Marcus, C. Schlenker, I. Sheikin, and D. Vignolles, Eur. Phys. J. B **58**, 25 (2007).

[12] D. Andres, M. V. Kartsovnik, W. Biberacherm, K. Neumaier, I. Sheikn, H. Muller, and N. D. Kushch, Low Temp. Phys. **37**, 762 (2011).

[13] J. F. Wang, M. Yang, L. Li, M. Sasaki, A. Ohnishi, M. Kitaura, K. S. Kim, and H. J. Kim, Phys. Rev. B **89**, 035137 (2014).

[14] M. Sasaki, N. Miyajima, W. X. Gao, H. Negishi, H. Kadomatsu, and M. Inoue, Synth. Met. **103**, 2660 (1999).

[15] M. Inoue, G. Machel, I. Laue, M. V. Ortenberg, and M. Sasaki, Phys. Status Solidi B **172**, 431 (1992).

[16] M. Sasaki, Y. Hara, M. Inoue, T. Takamasu, N. Miura, G. Machel, and M. von Ortenberg, Phys. Rev. B. **55**, 4983 (1997).

[17] M. Sasaki, N. Miyajima, H. Negishi, W. X. Gao, M. Inoue, H. Kadomatsu, G. Machel, H. Nojiri, and M. Matokawa, J. Phys. Soc. Jpn. **68**, 539 (1999).

[18] S. Hill, S. Uji, M. Takashita, C. Terakura, T. Terashima, H. Aoki, J. S. Brooks, Z. Fisk, and J. Sarrao, Phys. Rev. B **58**, 10778 (1998).

[19] K. I. Suga, N. Miyajima, M. Sasaki, and K. Kindo, Physica E (Amsterdam, Neth.) **18**, 136 (2003).

[20] M. Sasaki, N. Miyajima, H. Negishi, K. Suga, Y. Narumi, and K. Kindo, Physica B (Amsterdam, Neth.) **298**, 520 (2001).

[21] M. Sasaki, M. Inoue, N. Miyajima, Y. Mishima, and H. Negishi, Physica B (Amsterdam, Neth.) **284–288**, 1720 (2000).

[22] L. Kihlborg, Acta Chem. Scand. **13**, 954 (1959).

[23] R. Knorr and U. Müller, Z. Anorg. Allg. Chem. **621**, 541 (1995).

[24] N. Hiraoka, T. Buslaps, V. Honkimäki, H. Guyot, and C. Schlenker, Phys. Rev. B **71**, 125417 (2005).

[25] E. Canadell, M. H. Whangbo, C. Schlenker, and C. Escribe-Filipppini, Inorg. Chem. **28**, 1466 (1989).

[26] S. Hill, S. Valfells, S. Uji, J. S. Brooks, G. J. Athas, P. S. Sandhu, J. Sarrao, Z. Fisk, J. Geoette, H. Aoki, and T. Terashima, Phys. Rev. B **55**, 2018 (1997).

[27] S. Ohara, H. Negishi, and M. Inoue, Phys. Status Solidi B **172**, 419 (1992).

[28] K. I. Suga, A. Ohnishi, M. Koyano, M. Sasaki, and K. Kindo, J. Phys. Soc. Jpn. **77**, 074605 (2008).

[29] G. H. Gweon, S. K. Mo, J. W. Allen, C. R. Ast, H. Höchst, J. L. Sarrao, and Z. Fisk, Phys. Rev. B **72**, 035126 (2005).

[30] C. Proust, R. Yagi, A. Kawasumi, A. Kovalev, D. Vignolles, M. Kartsovnik, L. Brossard, and N. Kushch, Phys. Rev. B **62**, 2388 (2000).

[31] F. L. Pratt, J. Singleton, M. Doporto, A. J. Fisher, T. J. B. M. Janssen, J. A. A. J. Perenboom, M. Kurmoo, W. Hayes, and P. Day, Phys. Rev. B **45**, 13904 (1992).

[32] T. Osada, R. Yagi, A. Kawasumi, S. Kagoshima, N. Miura, M. Oshima, and G. Saito, Phys. Rev. B **41**, 5428 (1990).

[33] J. Z. Ke, M. Yang, H. K. Zuo, H. P. Zhu, C. B. Liu, R. Chen, C. Dong, W. X. Liu, M. Y. Shi, and J. F. Wang, J. Alloys Compd. **835**, 155417 (2020).

[34] See Supplemental Material at http://link.aps.org/supplemental/10.1103/PhysRevB.102.245135 for temperature dependence resistivity under different magnetic field and angle-dependent in-plane magnetoresistance with magnetic field up to 59 T.

[35] R. H. McKenzie, arXiv:cond-mat/9706235.

[36] J. Dumas, H. Guyot, H. Balaska, J. Marcus, D. Vignolles, I. Sheikin, A. Audouard, L. Brossard, and C. Schlenker, Physica B (Amsterdam, Neth.) **346-347**, 314 (2004).

[37] L. Balicas, G. Kriza, and F. I. B. Williams, Phys. Rev. Lett. **75**, 2000 (1995).

[38] S. Uji, T. Terashima, H. Aoki, J. S. Brooks, M. Tokumoto, S. Takasaki, J. Yamada, and H. Anzai, Phys. Rev. B **53**, 14399 (1996).

[39] T. Takamasu, H. Ochimizu, and N. Miura, Physica B (Amsterdam, Neth.) **184**, 327 (1993).

[40] D. Shoenberg, *Magnetic Oscillations in Metals* (Cambridge University Press, Cambridge, UK, 1984).

[41] N. W. Ashcroft and N. D. Mermin, *Solid State Physics* (Holt, Rinehart and Winston, New York, 1976).

[42] M. Sasaki, G. X. Tai, S. Tamura, and M. Inoue, Phys. Rev. B **47**, 6216 (1993).

[43] R. W. Stark and C. B. Friedberg, J. Low Temp. Phys. **14**, 111 (1974).

[44] N. P. Breznay, I. M. Hayes, B. J. Ramshaw, R. D. Mcdonald, Y. Krockenberger, A. Ikeda, H. Irie, H. Yamamoto, and J. G. Analytis, Phys. Rev. B **94**, 104514 (2016).

[45] S. Uji, J. S. Brooks, M. Chaparala, S. Takasaki, J. Yamada, and H. Anzai, Phys. Rev. Lett. **55**, 12446 (1997).
[46] A. A. House, N. Harrison, S. J. Blundell, I. Deckers, J. Singleton, F. Herlach, W. Hayes, J. A. A. J. Perenboom, M. Kurmoo, and P. Day, Phys. Rev. B **53**, 9127 (1996).
[47] Y. J. Jo, L. Balicas, C. Capan, K. Behnia, P. Lejay, J. Flouquet, J. A. Mydosh, and P. Schlottmann, Phys. Rev. Lett. **98**, 166404 (2007).
[48] G. W. Scheerer, W. Knafo, D. Aoki, G. Ballon, A. Mari, D. Vignolles, and J. Flouquet, Phys. Rev. B **85**, 094402 (2012).
[49] Y. J. Wang, Y. J. Wang, J. H. Yu, Y. Q. Wang, C. Y. Xi, L. S. Ling, S. L. Zhang, J. R. Wang, Y. M. Xiong, T. Han, H. Han, J. Yang, J. X. Gong, L. Luo, W. Tong, L. Zhang, Z. Qu, Y. Y. Han, W. K. Zhu, L. Pi, X. G. Wan, C. J. Zhang and Y. H. Zhang, Phys. Rev. B **97**, 115133 (2018).
[50] A. K. R. Briffa, E. Blackburn, S. M. Hayden, E. A. Yelland, M. W. Long, and E. M. Forgan, Phys. Rev. B **93**, 094502 (2016).
[51] G. Montambaux, Phys. Rev. B **38**, 4788 (1988).
[52] A. M. Clogston, Phys. Rev. Lett. **9**, 266 (1962).
[53] J. S. Qualls, L. Balicas, J. S. Brooks, N. Harrison, L. K. Montgomery, and M. Tokumoto, Phys. Rev. B **62**, 10008 (2000).
[54] C. A. Balseiro and L. M. Falicov, Phys. Rev. B **34**, 863 (1985).